Supplementary Information

In-memory Ferroelectric Differentiator

Guangdi Feng[1,2,#], Xiaoming Zhao[1,#], Xiaoyue Huang[1,#], Xiaoxu Zhang[1], Yangyang Wang[1], Wei Li[1], Luqiu Chen[1], Shenglan Hao[1], Qiuxiang Zhu[1], Yachin Ivry[3], Brahim Dkhil[4], Bobo Tian[1,2,*], Peng Zhou[5,*], Junhao Chu[1,6], Chungang Duan[1,7,*]

[1] Key Laboratory of Polar Materials and Device, Ministry of Education, Shanghai Center of Brain-inspired Intelligent Materials and Devices, Department of Electronics, East China Normal University, Shanghai 200241, China.

[2] Chongqing Key Laboratory of Precision Optics, Chongqing Institute of East China Normal University, Chongqing 401120, China.

[3] Department of Materials Science and Engineering, Solid-State Institute, Technion-Israel Institute of Technology, Haifa, 3200003 Israel.

[4] Université Paris-Saclay, CentraleSupélec, CNRS-UMR8580, Laboratoire SPMS, 91190 Gif-sur-Yvette, France.

[5] State Key Laboratory of Integrated Chip and Systems, School of Microelectronics, Frontier Institute of Chip and System, Fudan University, Shanghai 200433, China

[6] Institute of Optoelectronics, Shanghai Frontier Base of Intelligent Optoelectronics and Perception, Fudan University, Shanghai 200438, China

[7] Collaborative Innovation Center of Extreme Optics, Shanxi University, Shanxi 030006, China.

[#] These authors contributed equally

[*] Email: bbtian@ee.ecnu.edu.cn, pengzhou@fudan.edu.cn and cgduan@clpm.ecnu.edu.cn

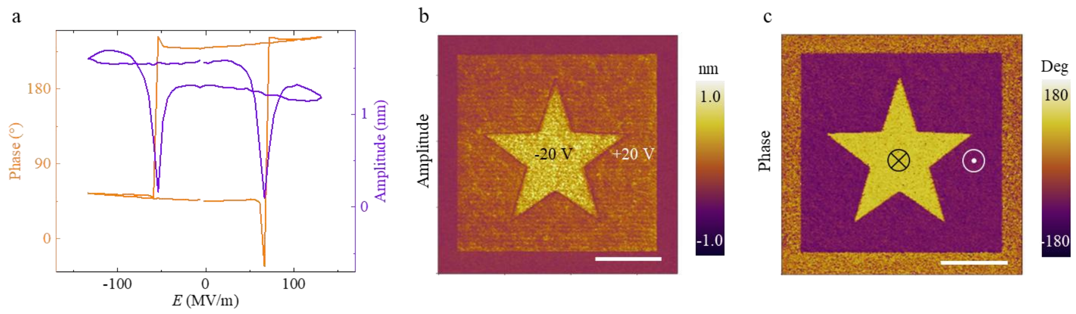

Figure S1. a-c, The piezoelectric force microscope (PFM) phase and amplitude hysteresis loops (**a**), PFM amplitude image (**b**) and PFM phase image (**c**) of a 200-nm thick ferroelectric polymer films. The films are polarized by +20 V on 15×15 μm^2 and -20 V on an inner star area. The scale bar is 3 μm. Source data of (**a**) are provided as a Source Data file.

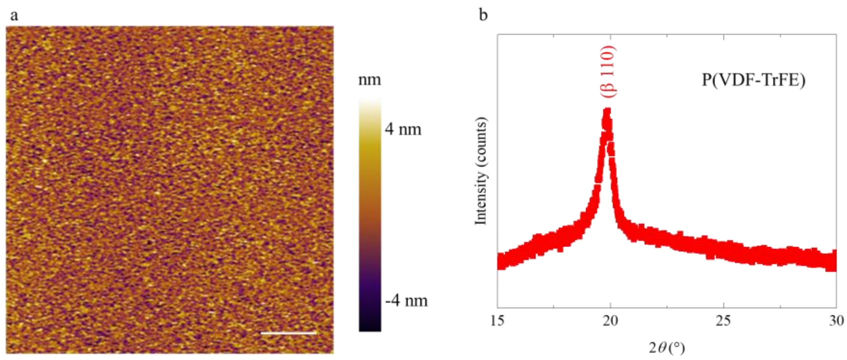

Figure S2. a, The topography and crystalline phase of P(VDF-TrFE) films. **a**, The atomic force microscope topography image of the P(VDF-TrFE) films. The surface has a low average roughness of 1.25 nm across a 30×30 μm2 area. The scale bar is 5 μm. **b**, The X-ray diffraction (XRD) of P(VDF-TrFE) films. Source data of (**b**) are provided as a Source Data file.

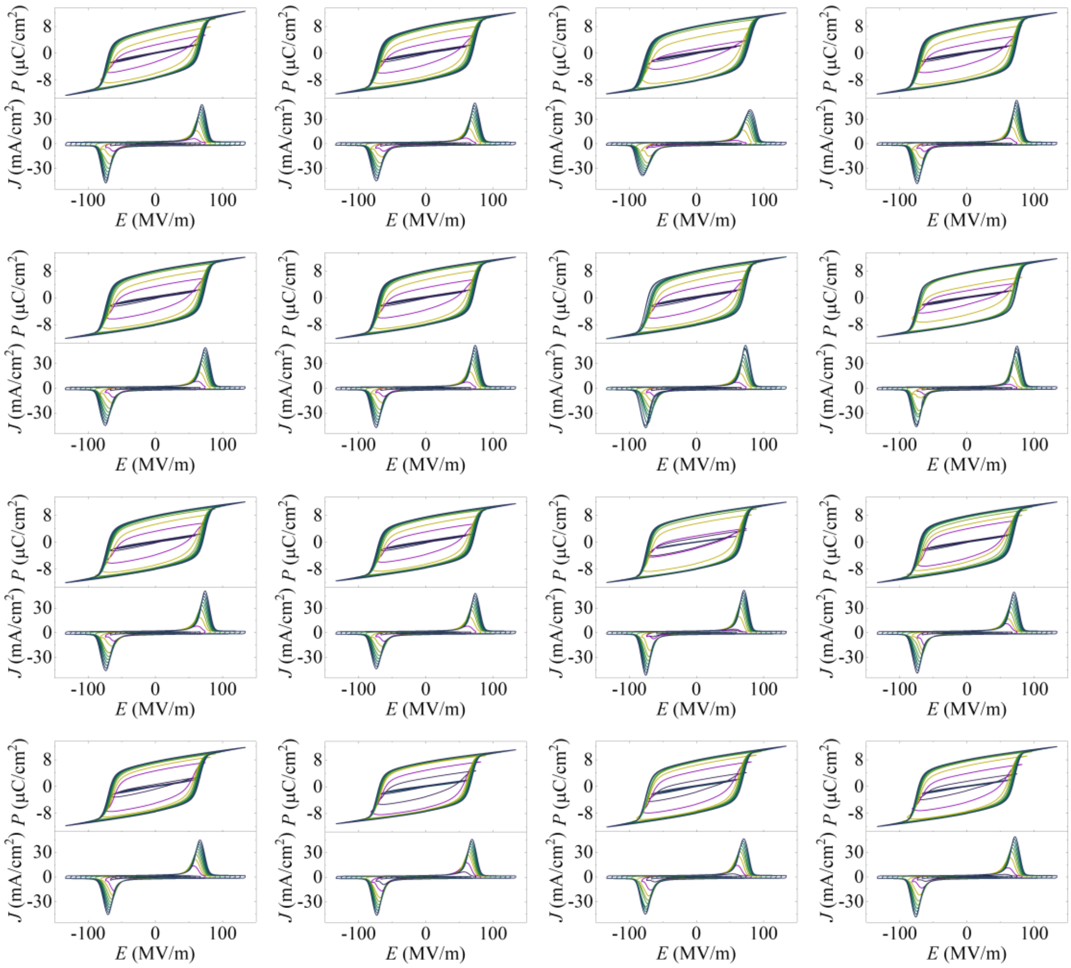

Figure S3. The multiple polarization versus electric field (*P*-*E*) hysteresis loops (up panel) and current density versus electric field (*J*-*E*) hysteresis loops (bottom panel) of 16 typical ferroelectric P(VDF-TrFE) capacitors. Source data are provided as a Source Data file.

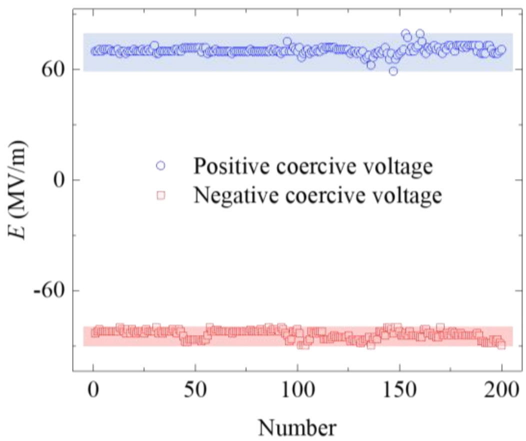

Figure S4. The coercive field distribution of 200 sampled units from the ferroelectric capacitor crossbar array. Source data are provided as a Source Data file.

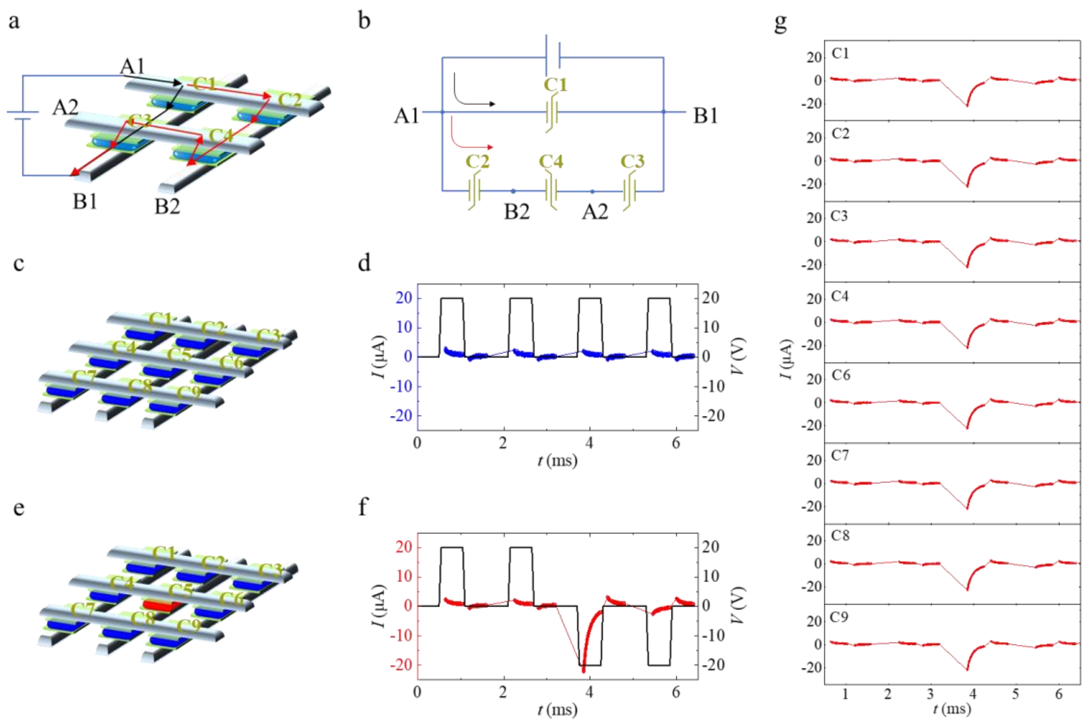

Figure S5. a, The sneak-path issue in the ferroelectric capacitor crossbar array structure. **b**, The equivalent circuit of the sneak-path issue. **c**, The polarization state (downward, color blue) of nine capacitors (C1-C9). **d**, The evolution of transient currents under voltage pulse (+20V, 5μs) sequence applied to the ferroelectric capacitors to tune the polarization state of (C1-C9). **e-f**, The capacitor (C5) is tuned into polarization upward (color red) (**e**) after suffering voltage pulse sequence: two positive voltage pulse (+20 V, 5μs) followed by the opposite two (−20 V, 5μs) (**f**). **g**, The evolution of transient currents of capacitors except C5 by suffering the same voltage pulse sequence as in (**f**). Source data of (**d**), (**f**) and (**g**) are provided as a Source Data file.

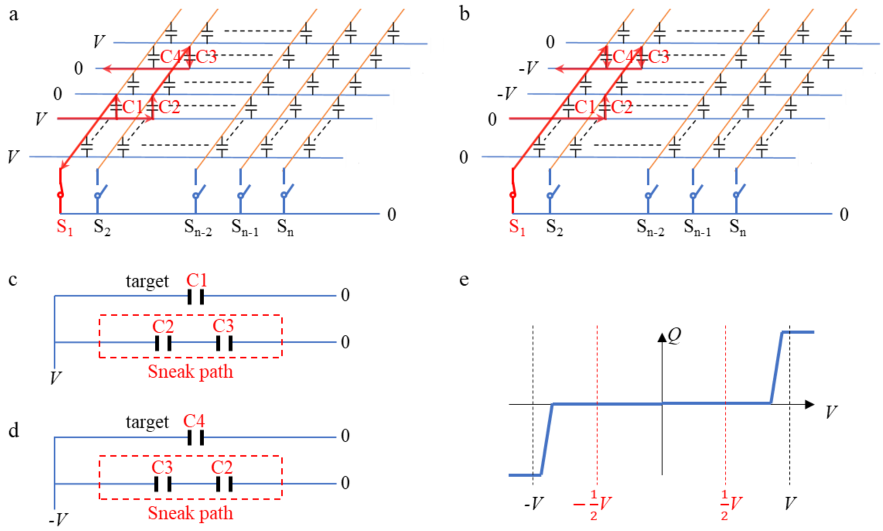

Figure S6 The programming process in the ferroelectric capacitor crossbar array. **a-b**, The schematic of positive (**a**) and negative (**b**) voltage pulses are input into the ferroelectric capacitor crossbar array to align the polarization of target cells upward and downward respectively. **c**, The equivalent circuit of target path and one of sneak path in (**a**). **d**, The equivalent circuit of target path and one of sneak path in (**b**). **e**, The schematic of how the nonlinear domain switching results in the ferroelectric capacitor crossbar array disturb immunity.

Supplementary note 1

As sketched in **Fig. S5a**, when we intend to apply a voltage (V) between A1 and B1 lines to operate the target C1 cell, the path highlighted by black arrow is the desired current path. However, current could also un-intentionally flow through the red path which is called the sneak path current. The equivalent circuit of the sneak-path is shown in **Fig. S5b**. Note that, while C1 cell suffers the whole V voltage, the C2, C4 and C3 in the sneak path, having a same value of capacitance, suffer V/3, -V/3 and V/3, respectively. This is fundamentally different from the scenario in a resistive crossbar, where the neighboring unselected cell in the high-resistance state suffers mostly V in the sneak path, which will trigger error operation without a protection of selecting circuit. Because of the exist of V_C in ferroelectric capacitors, by choosing an appropriate voltage satisfying V > V_C and V/2 < V_C, it is expected that the ferroelectric capacitor array has good immunity to the sneak path issue.

A region of 3×3 cells in a 40×40 ferroelectric capacitor array is randomly picked to investigate its immunity to sneak path issue (**Fig. S5c**). Firstly, four positive voltage pulses (+20 V, 5μs) are applied to all capacitors (C1-C9) in turn, the absence of current peak (**Fig. S5d)** implies that ferroelectric domains in C1-C9 are downward (depicted by blue color in **Fig. S5c**). Then two positive voltage pulses (+20 V, 5μs) followed by two negative voltage pulses (-20 V, 5μs) are applied to C5. No current peak is observed during the former two positive voltage pulses, implying the robust maintenance of downward domains in C5 which is not affected by operations in neighboring cells. The clear negative current peak appearing accompanying the first negative voltage pulse confirms the polarization reversal from downward domains to upward domains. Other capacitors are also carefully checked with the two positive voltage pulses (+20 V, 0.5 ms) followed by two negative voltage pulses (-20 V, 0.5 ms), the uniform polarization reversals at the first negative voltage pulse for all capacitors (**Fig. S5g**) imply that reduplicative operations have almost no influences on the domain configuration in neighboring cells.

The passive capacitor crossbar array can also be programed column by column. As shown in **Figs. S6a-b**, the rows of the passive capacitor array are used as parallel inputs, and the columns are controlled ON and OFF by the matrix switch, which realizes parallel programming of specific column. **Figures S6a** and **b** sketch the programing process in which positive (**Fig. S6a**) and negative (**Fig. S6b**) voltage pulses are input into the ferroelectric capacitor crossbar array to align the polarization of target cells upward and downward respectively. Companying with the target path, there are sneak paths in a passive crossbar structure. To understand the disturb issue, equivalent circuits of a target path (C1 in **Fig. S6a**, C4 in **Fig. S6b**) and one of sneak path (C2 and C3 in **Fig. S6a**, C3 and C2 in **Fig. S6b**) are presented in **Figs. S6c-d**. We note that the applied voltage is shared by two capacitors (C2 and C3 in **Fig. S6a**, C3 and C2 in **Fig. S6b**) in sneak paths. Due to the nonlinear ferroelectric dynamics of P(VDF-TrFE), polarization switching only occurs when the input voltage is larger than the coercive voltage of ferroelectric films (**Fig. S6e**). The polarization switching hardly happen for these half-biased capacitors in sneak paths, resulting in the ferroelectric capacitor crossbar array disturb immunity. Thus, the domain configuration in the ferroelectric capacitor crossbar array can be precisely controlled.

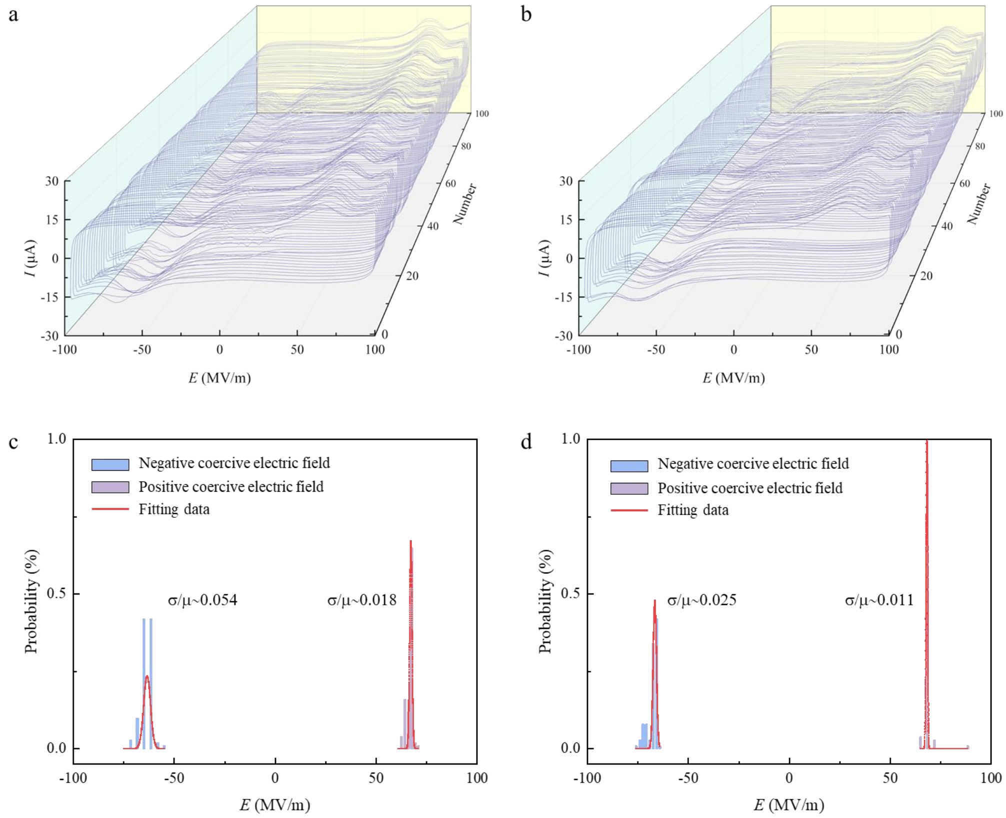

Figure S7. The uniformity of 40×40 capacitor crossbar array of two different batches. **a-b** The transient *I-V* curves of 100 random-selected capacitors for the array reproduced at first batch (**a**) and second batch (**b**) where transient current peaks correspond to ferroelectric coercive electric field. **c-d** The distribution of positive/negative coercive electric field of the 100 random-selected capacitors for the array reproduced at first batch (**c**) and second batch (**d**). Source data are provided as a Source Data file.

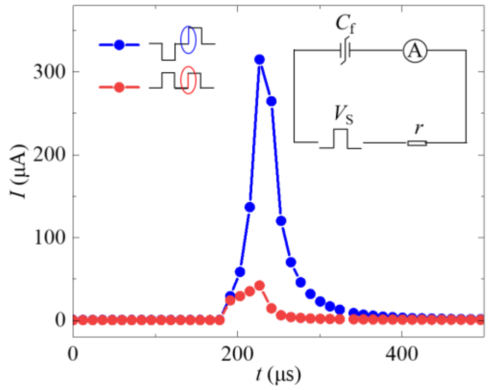

Figure S8. The transient current of a ferroelectric capacitor under the later stimuli of voltage pulses pair (20 V) with same polarity (red) and opposite polarity (blue). The high current peak during opposite voltage polarity is because of the ferroelectric domain switching while it only shows weak charging current for the one with the same polarity. Source data are provided as a Source Data file.

Supplementary note 2

When voltage pulse sequence with amplitude higher than the V_C is applied to the ferroelectric copolymer capacitor, if the former voltage pulse is negative, the positive voltage pulse triggers a large displacement current (blue color), including both the polarization reversal and charging effects. If the former voltage pulse is positive, the second positive voltage pulse gives a small displacement current (red color), including only the charging effect.

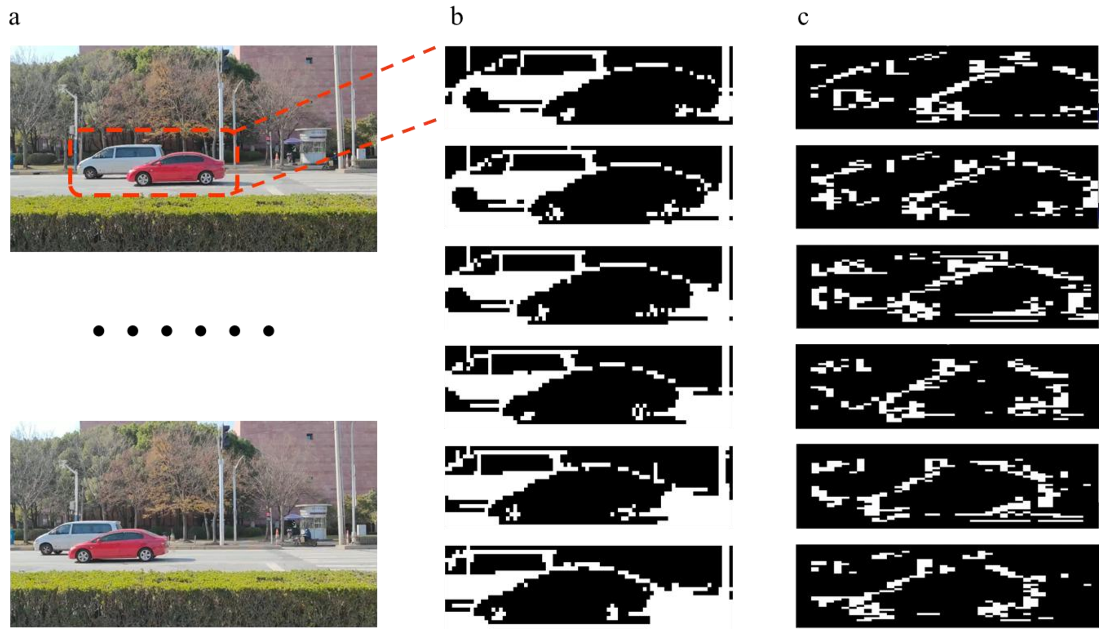

Figure S9. a, The moving vehicles image. **b,** Vehicles images are compressed and binarized to 40×160 pixels. **c,** The successful processing results of the moving car information using the voltage pulses with width of 2 μs and amplitude of 40 V.

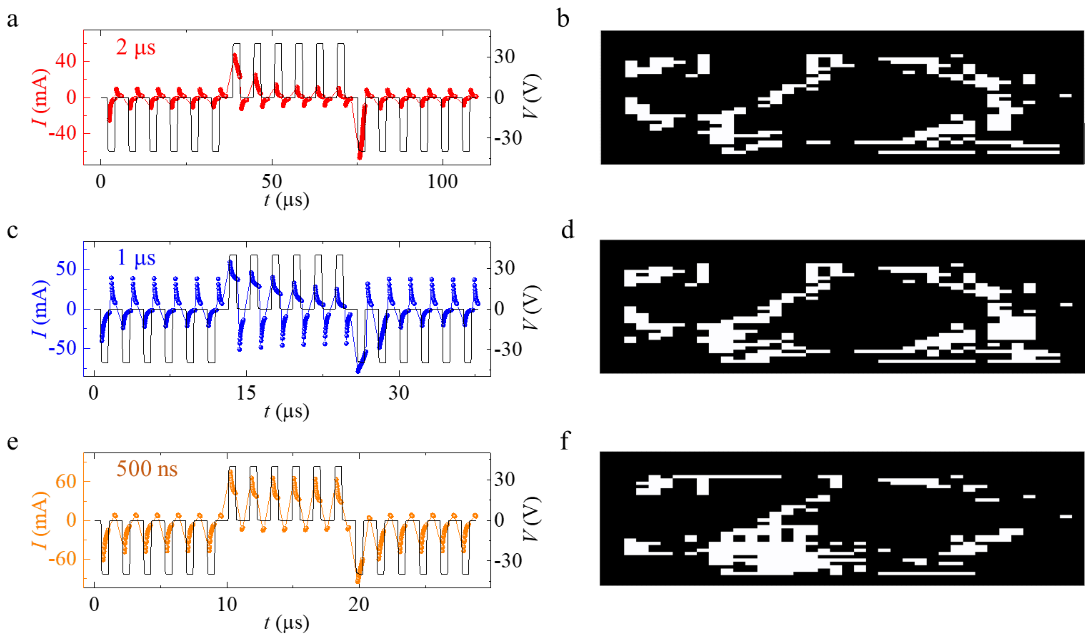

Figure S10. a, c, e, The evolution of transient currents over time under the voltage pulse sequence with a pulse width of 2 μs (**a**), 1 μs (**c**) and 500 ns (**e**) respectively. **b, d, f,** The processing results of the moving car information using the voltage pulses with width of 2 μs (**b**), 1 μs (**d**) and 500 ns (**f**) respectively. Source data of (**a**), (**c**) and (**e**) are provided as a Source Data file.

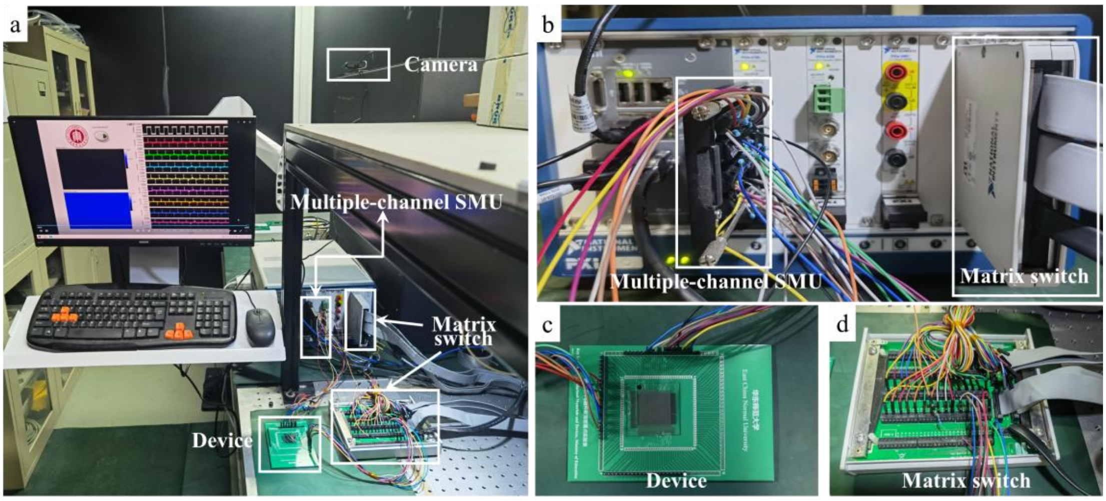

Figure S11. **a**, A real-time motion detecting system involving a camera to directly capture natural events, a ferroelectric capacitor array to single out motion information is designed, the Mutiple-channel of NI as read source is needed and voltage signals and transient currents are collected through sequentially unblocking the Matrix switch. **b-d,** The details of the Mutiple-channel of NI (**b**), the device of ferroelectric capacitor array (**c**) and the Matrix switch (**d**), respectively

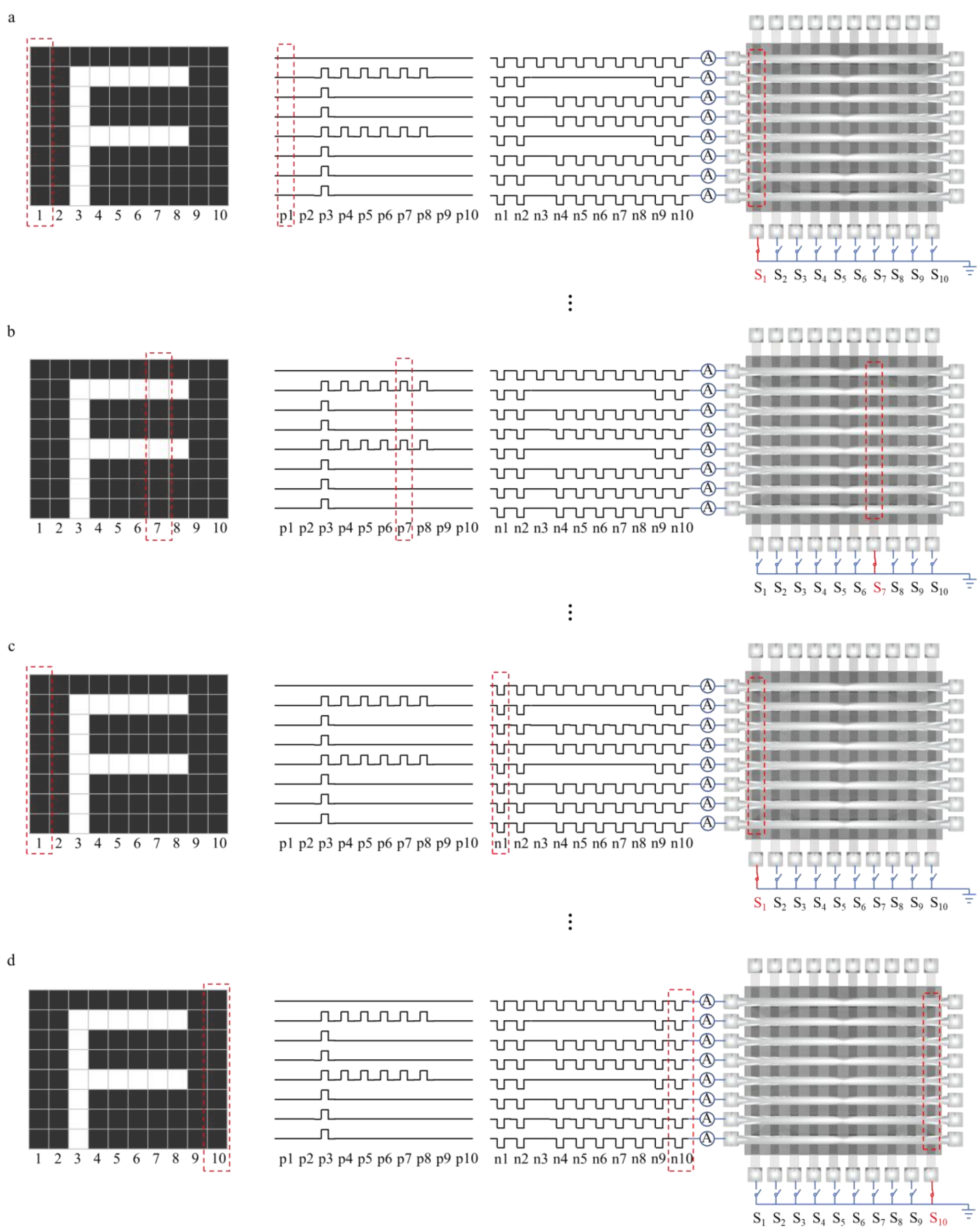

Figure S12. a-d, The flow chart showing how a 8×10-pixels "F" image is encoded by voltage pulse matrix and inputted to the ferroelectric capacitor crossbar array. To eliminate the disturbance by multi-operations, the white pixels and black pixels of the "F" image are separated and inputted into the array in sequence with a 1/2 voltage strategy. The white (black) pixels are encoded to positive (negative) voltage pulses (amplitude of 12 V, width of 0.06 s) while other pixels are encoded to zero voltage biases. These pixel voltage pulses are inputted into the ferroelectric capacitor crossbar array column by column to ensure that each pixel corresponds unique capacitor depending its location. A voltage pulse sequence with opposite polarity with pixel voltage are inputted to the column accordingly. For example, when p1-column (**a**), p7-column (**b**), n1-column (**c**) and n10-column (**d**) pixel voltage pulses are inputted into the ferroelectric capacitor crossbar array, the matrix switch S_1, S_7, S_1, S_{10} is turn on for receiving opposite 1/2 voltage, respectively.

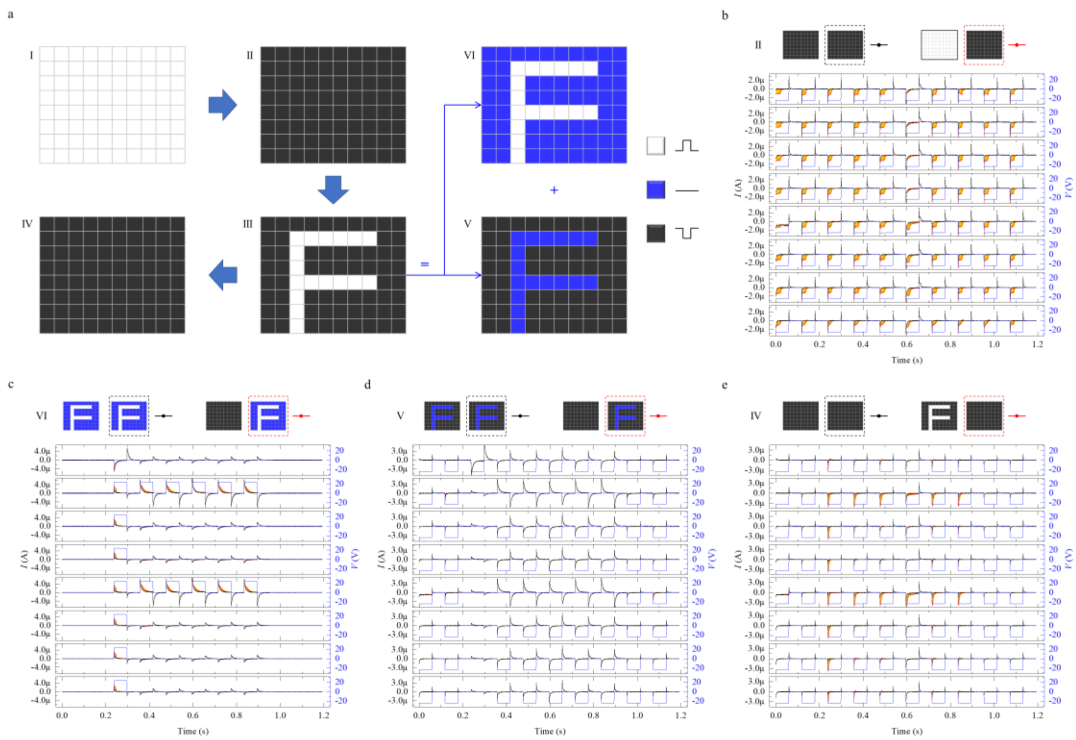

Figure S13. a, The test process of all-white-pixels, all-black-pixels, “F”-shape pixels and all-black-pixels images in turn. **b-e**, The evolution of transient currents during the inputting process of all-black-pixels image (**b**) that follows an all-white-pixels image (red) and all-black-pixels image that follows an all-black-piexls image (black), the white pixels of the “F”-shape-pixels image (**c**) that follows an all-black-pixels image (red) and the white pixels of the “F”-shape-pixels image that follows the white pixels of the “F”-shaped image (black), the black pixels of the “F”-shape-pixels image (**d**) that follows an all-black-pixels image (red) and the black pixels of the “F”-shape-pixels image that follows the black pixels of the “F”-shape-pixels image (black), all-black-pixels image (**e**) that follows “F”-shape-pixels image (red) and all-black-pixels image that follows an all-black-pixels image (black). Source data of (**b-e**) are provided as a Source Data file.

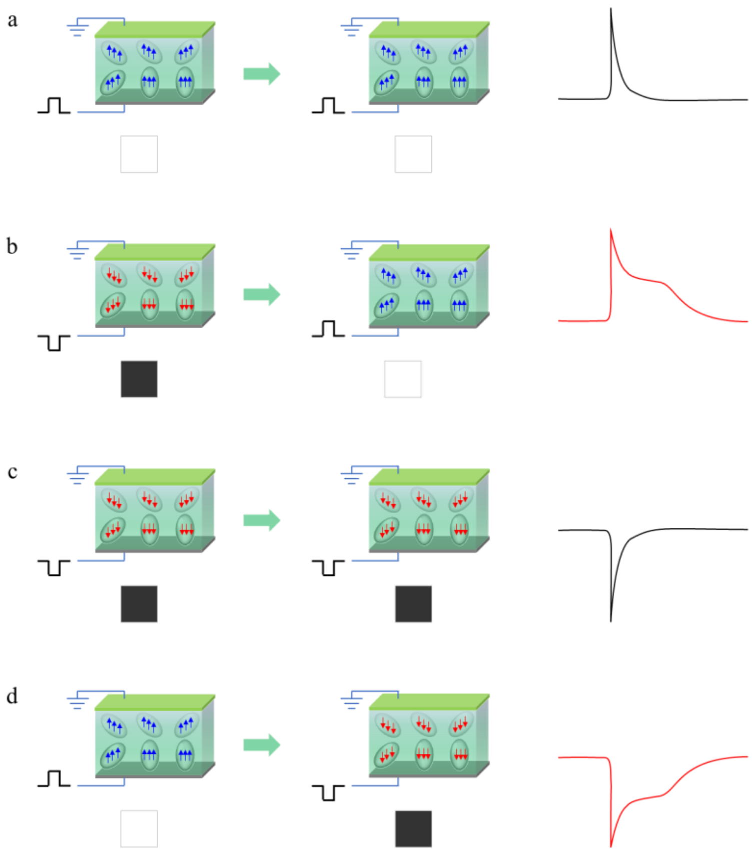

Figure S14 The evolution of ferroelectric domain with image pixels (polarity of pulses) and its transient currents under the fresh pulse.

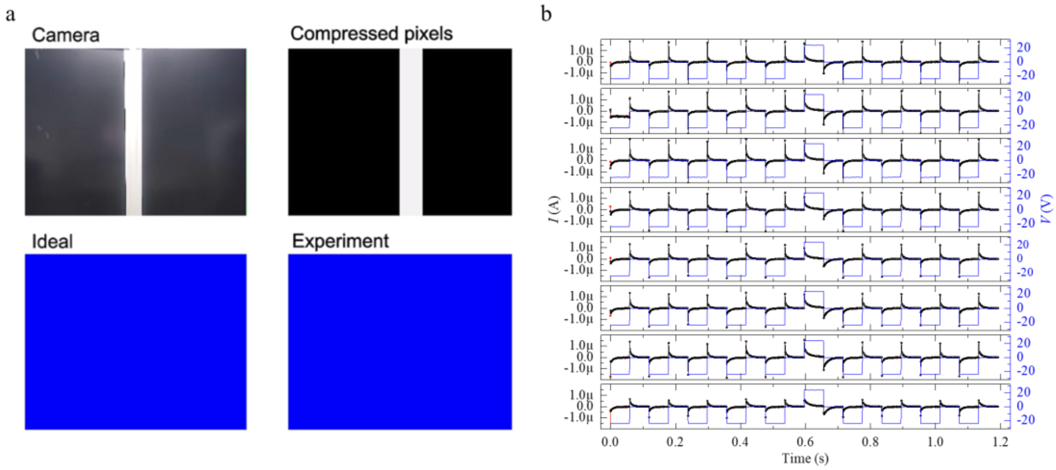

Figure S15. **a**, The first frame of image acquired by the camera, the compressed and binarized image, the motion pixels obtained from ideal differential operations and ferroelectric domain switching signals respectively. **b**, The evolution of transient currents during the inputting process of compressed pixels in (**a**). Source data of (**b**) are provided as a Source Data file.

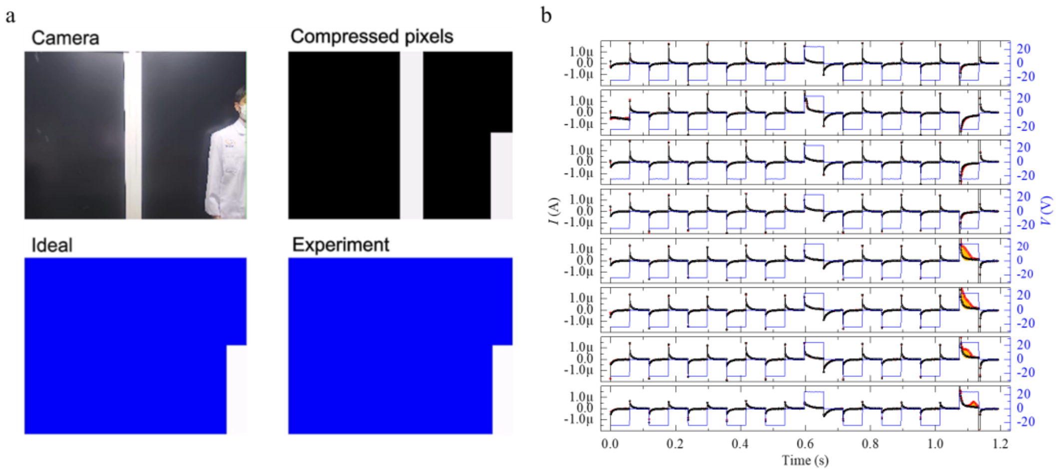

Figure S16. **a**, The second frame of image acquired by the camera, the compressed and binarized image, the motion pixels obtained from ideal differential operations and ferroelectric domain switching signals respectively. **b**, The evolution of transient currents during the inputting process of compressed pixels in (**a**). Source data of (**b**) are provided as a Source Data file.

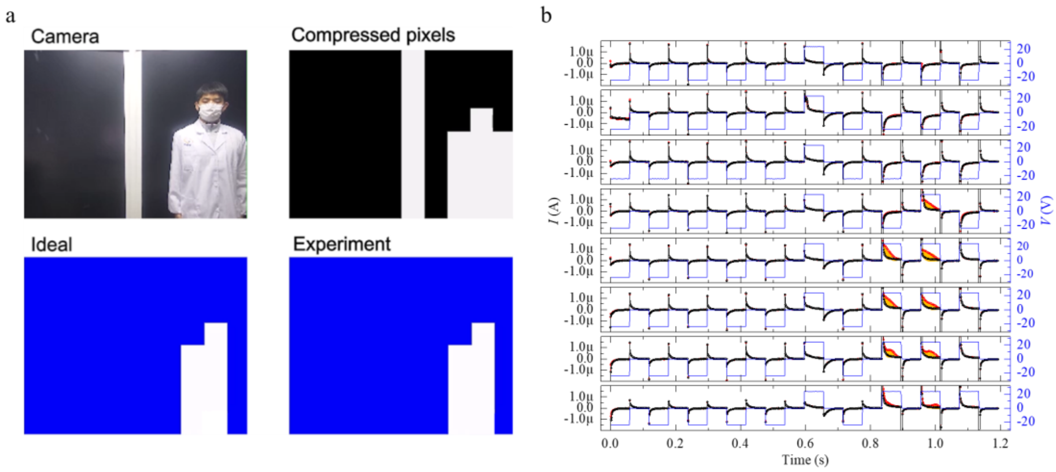

Figure S17. a, The third frame of image acquired by the camera, the compressed and binarized image, the motion pixels obtained from ideal differential operations and ferroelectric domain switching signals respectively. **b**, The evolution of transient currents during the inputting process of compressed pixels in (**a**). Source data of (**b**) are provided as a Source Data file.

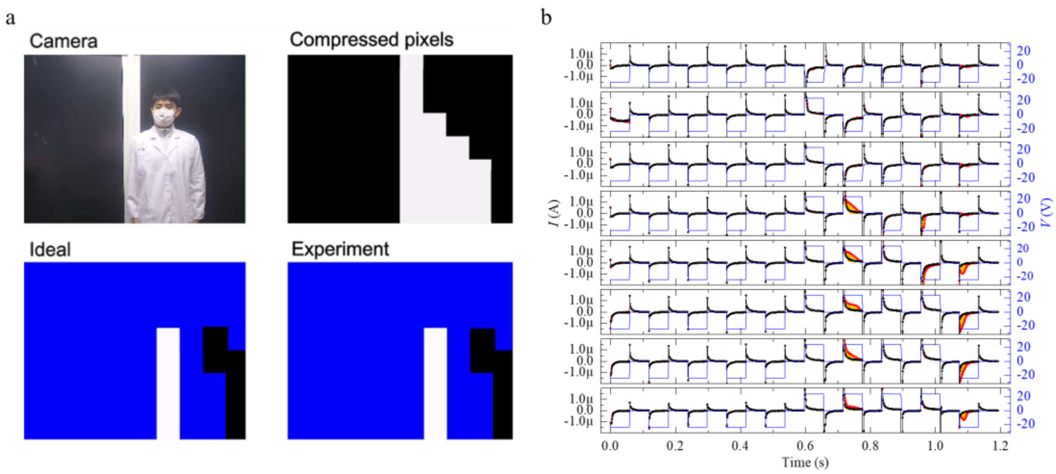

Figure S18. a, The 4th frame of image acquired by the camera, the compressed and binarized image, the motion pixels obtained from ideal differential operations and ferroelectric domain switching signals respectively. **b**, The evolution of transient currents during the inputting process of compressed pixels in (**a**). Source data of (**b**) are provided as a Source Data file.

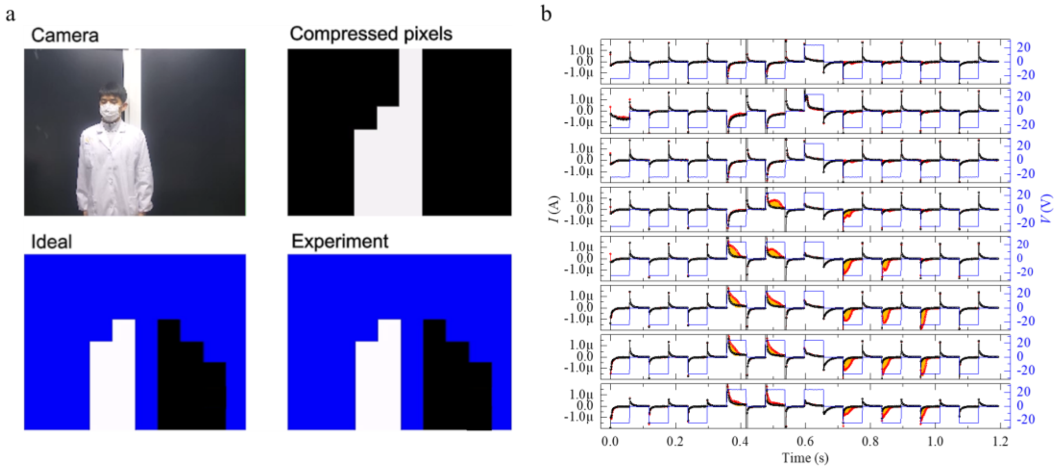

Figure S19. a, The 5th frame of image acquired by the camera, the compressed and binarized image, the motion pixels obtained from ideal differential operations and ferroelectric domain switching signals respectively. **b**, The evolution of transient currents during the inputting process of compressed pixels in (**a**). Source data of (**b**) are provided as a Source Data file.

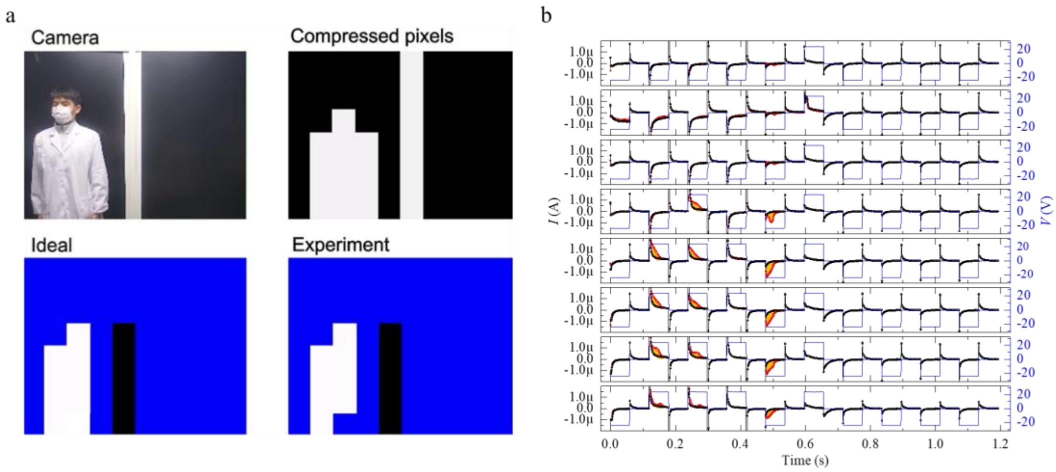

Figure S20. a, The 6th frame of image acquired by the camera, the compressed and binarized image, the motion pixels obtained from ideal differential operations and ferroelectric domain switching signals respectively. **b**, The evolution of transient currents during the inputting process of compressed pixels in (**a**). Source data of (**b**) are provided as a Source Data file.

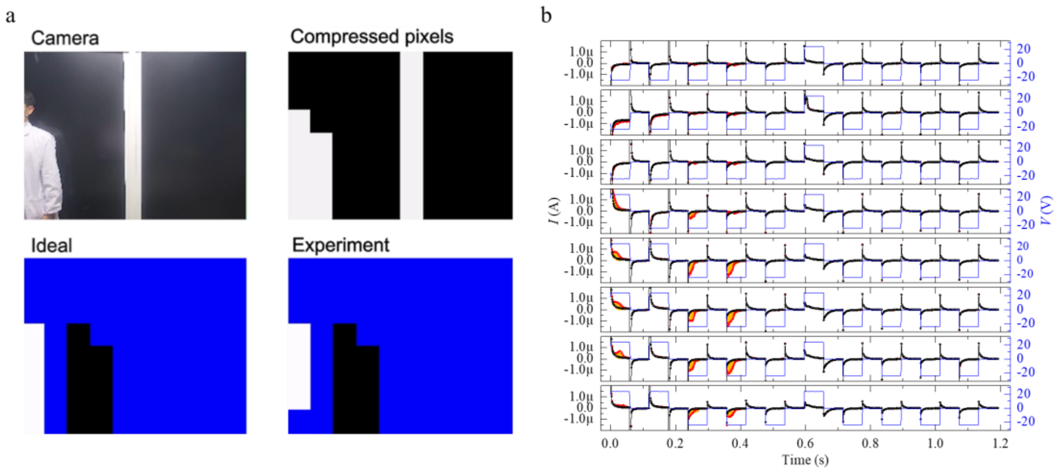

Figure S21. **a**, The 7th frame of image acquired by the camera, the compressed and binarized image, the motion pixels obtained from ideal differential operations and ferroelectric domain switching signals respectively. **b**, The evolution of transient currents during the inputting process of compressed pixels in (**a**). Source data of (**b**) are provided as a Source Data file.

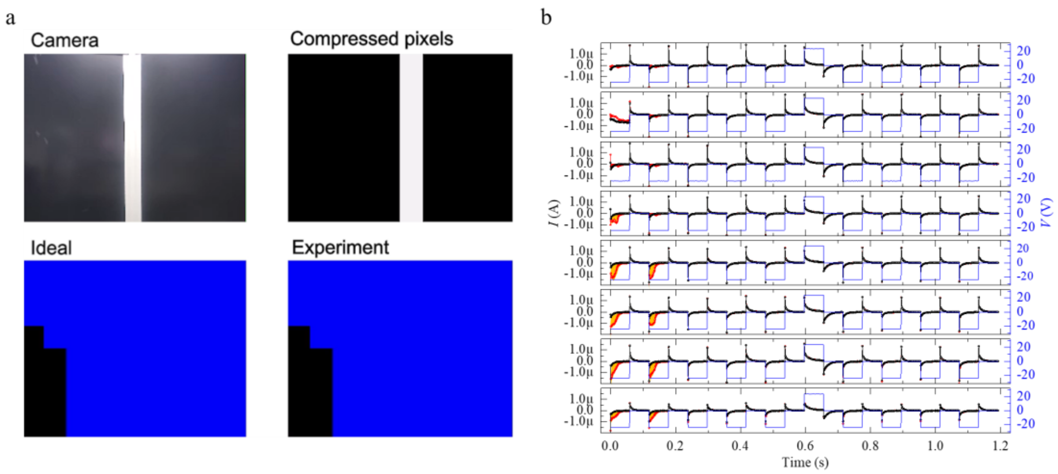

Figure S22. **a**, The 8th frame of image acquired by the camera, the compressed and binarized image, the motion pixels obtained from ideal differential operations and ferroelectric domain switching signals respectively. **b**, The evolution of transient currents during the inputting process of compressed pixels in (**a**). Source data of (**b**) are provided as a Source Data file.

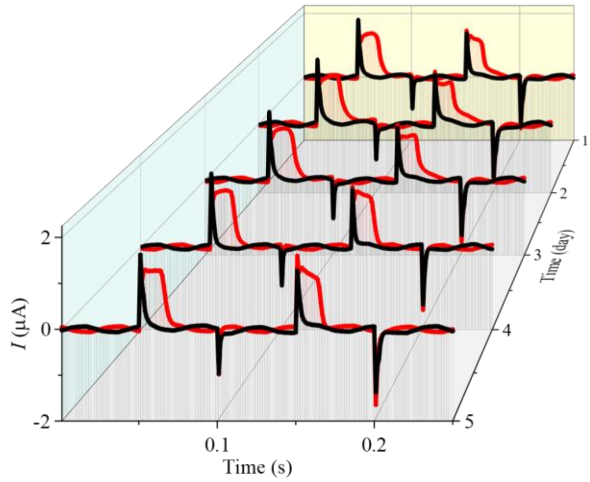

Figure S23 The retention property of the ferroelectric capacitors. Source data are provided as a Source Data file.

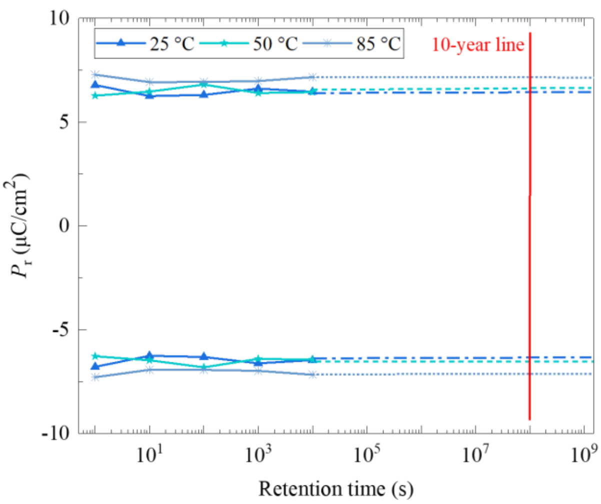

Figure S24 The polarization retention capability of P(VDF-TrFE) capacitors under temperature of 25 °C, 50 °C and 85 °C respectively. Source data are provided as a Source Data file.

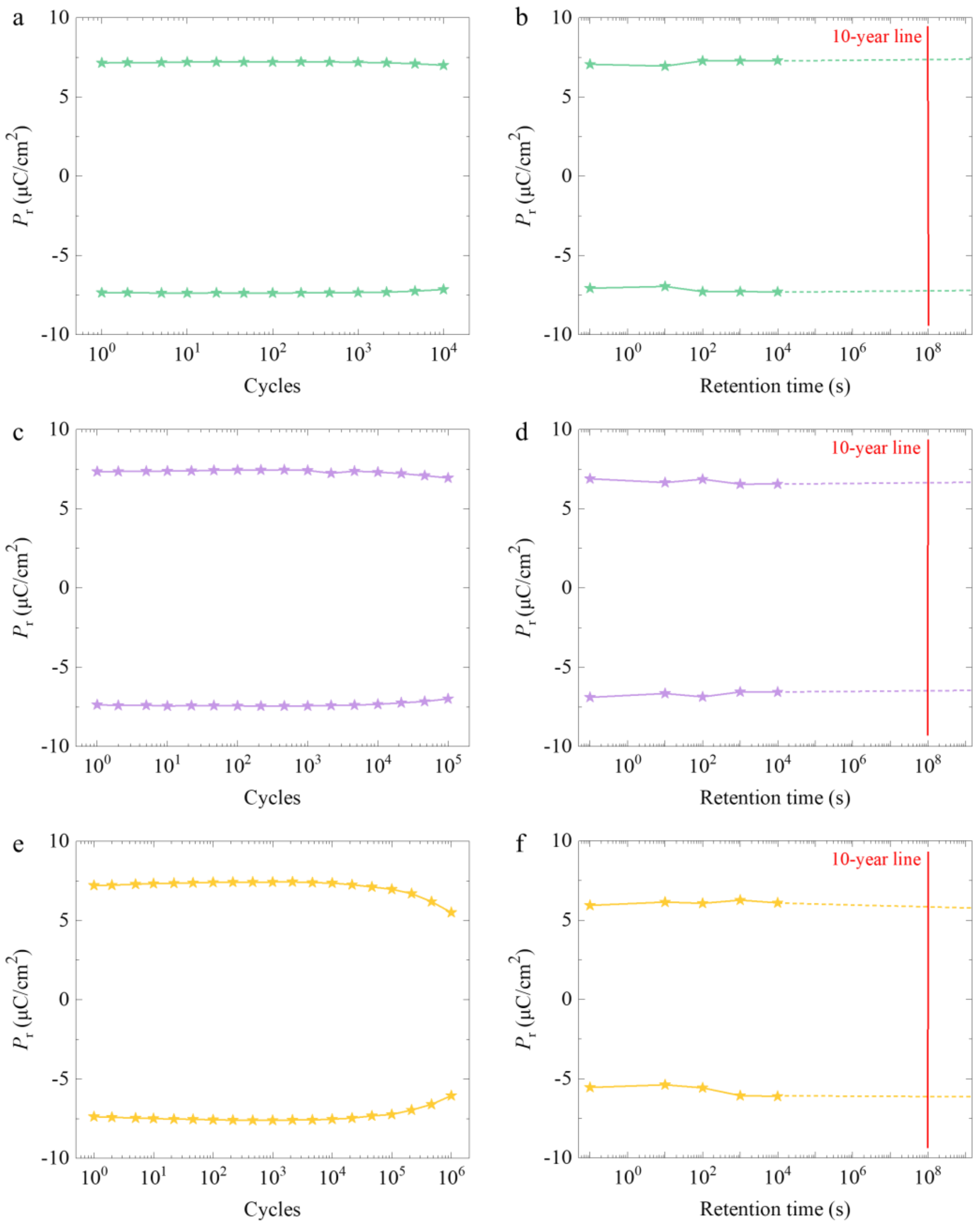

Figure S25 The polarization retention capability of P(VDF-TrFE) capacitors after device aging temperature of 10^4 cycles, 10^5 cycles and 10^6 cycles respectively. Source data are provided as a Source Data file.

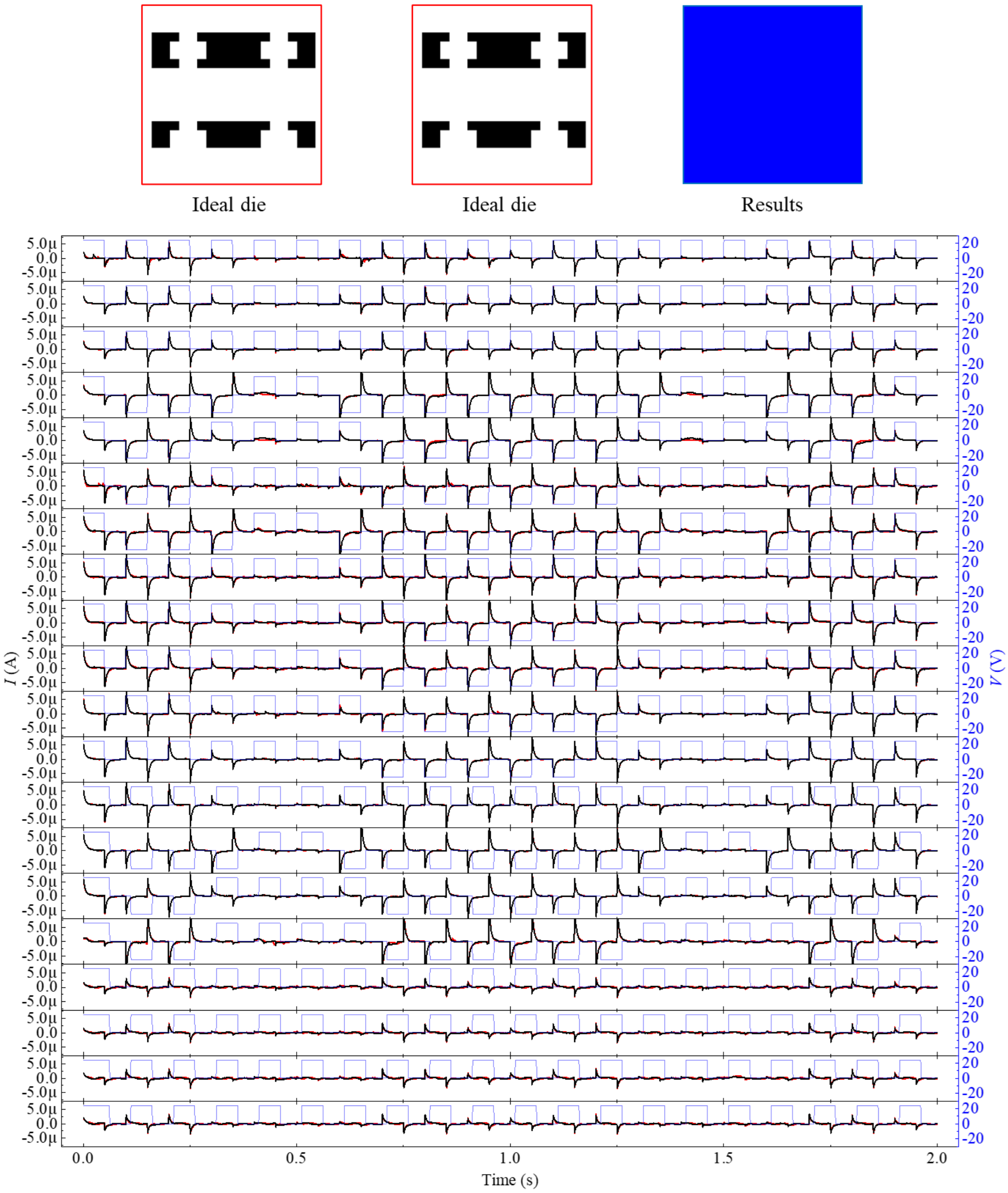

Figure S26. The evolution of transient currents during the inputting process of an ideal die image that follows an ideal die image. Source data are provided as a Source Data file.

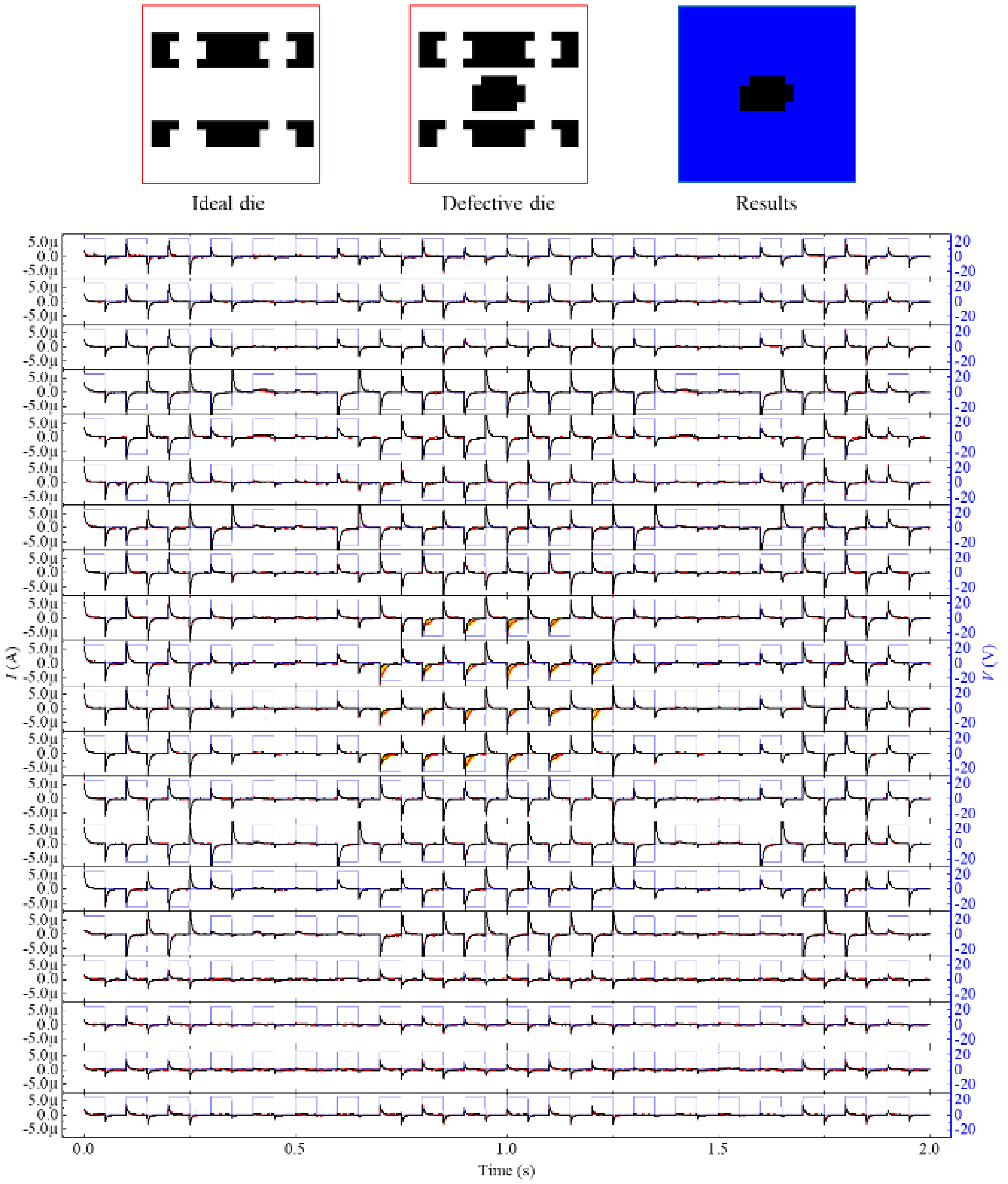

Figure S27. The evolution of transient currents during the inputting process of an ideal die image that follows a defective die image. Source data are provided as a Source Data file.

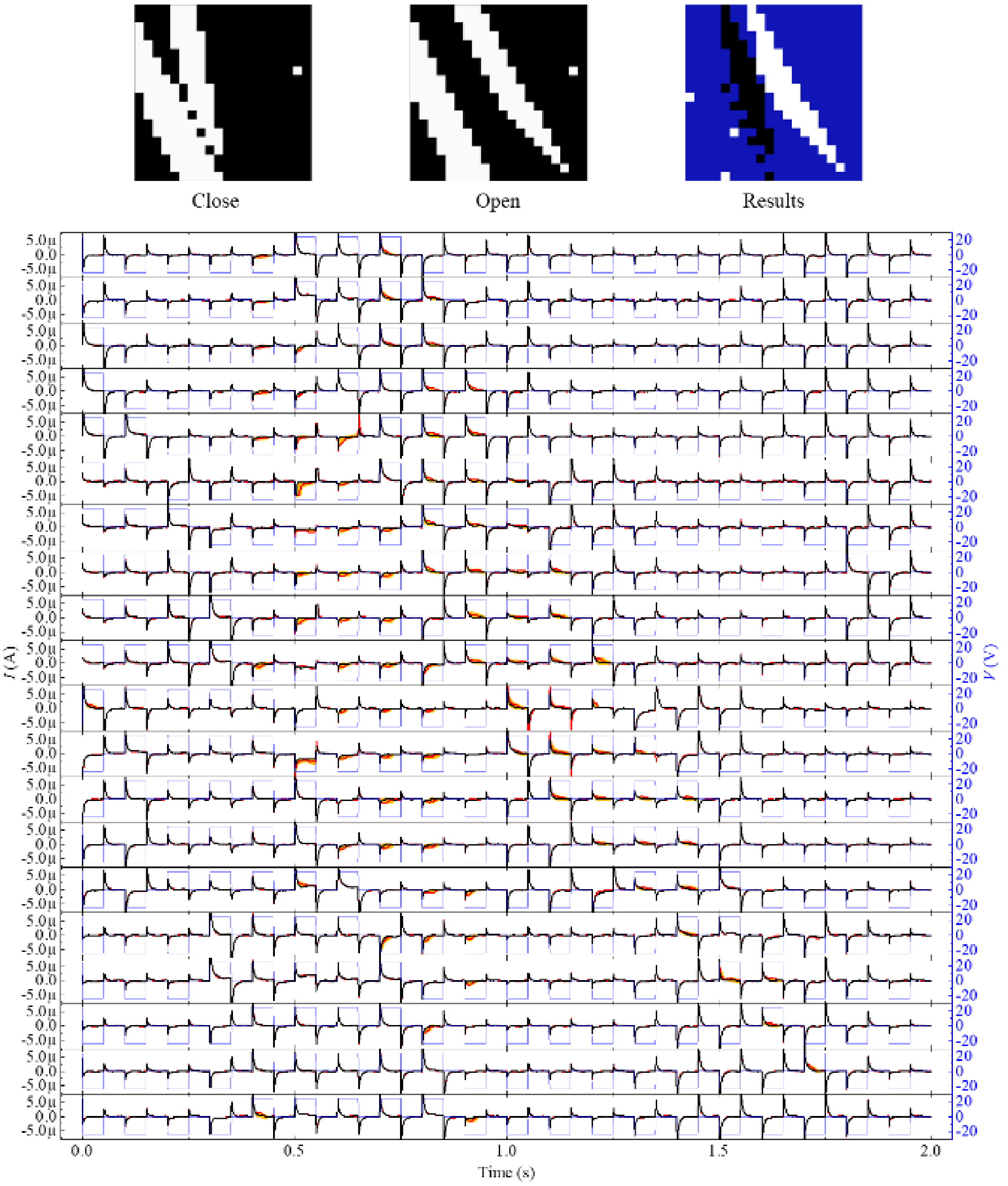

Figure S28. The evolution of transient currents during the inputting process of a closed switch image that follows an open switch image. Source data are provided as a Source Data file.

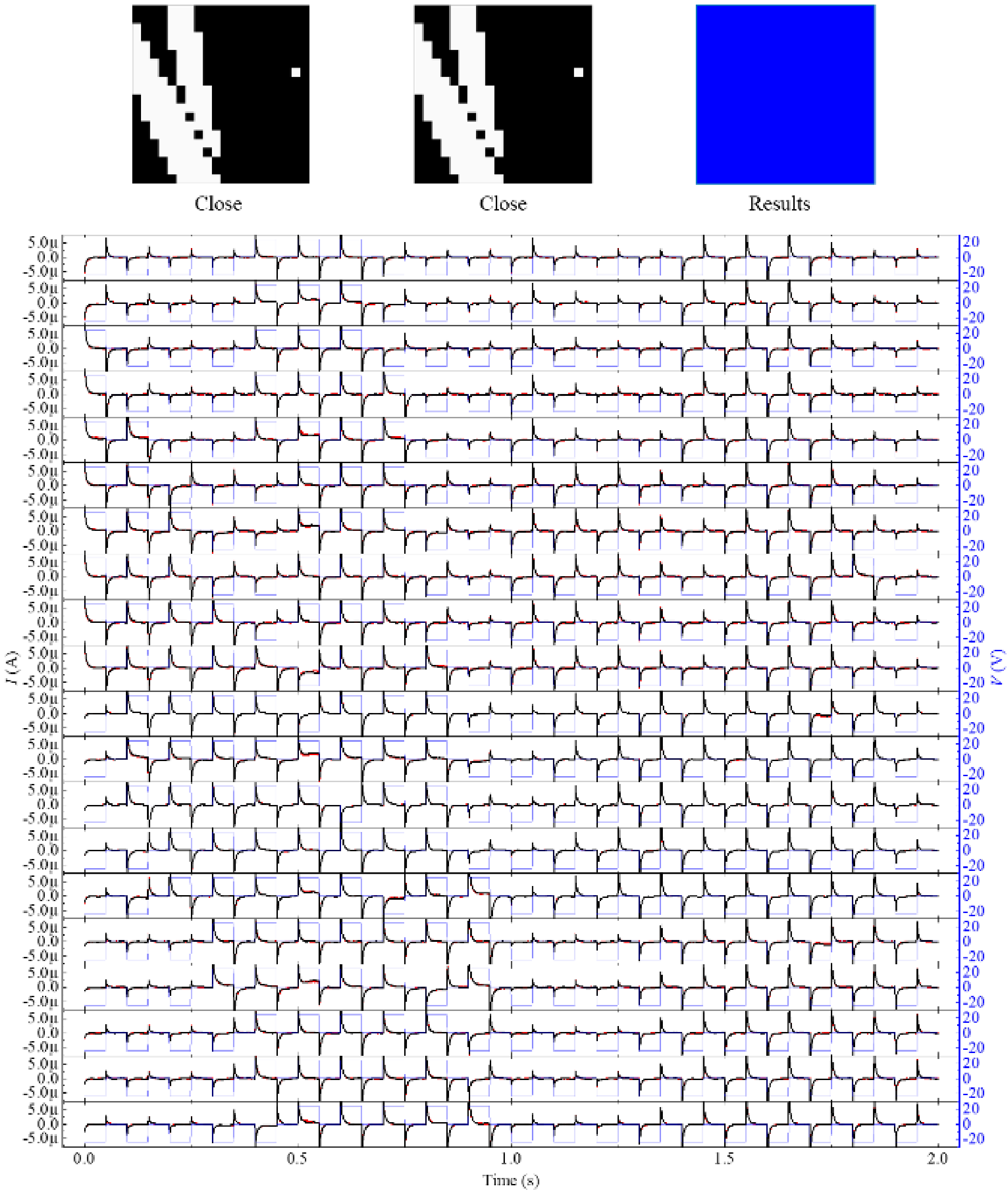

Figure S29. The evolution of transient currents during the inputting process of a closed switch image that follows a closed switch image. Source data are provided as a Source Data file.

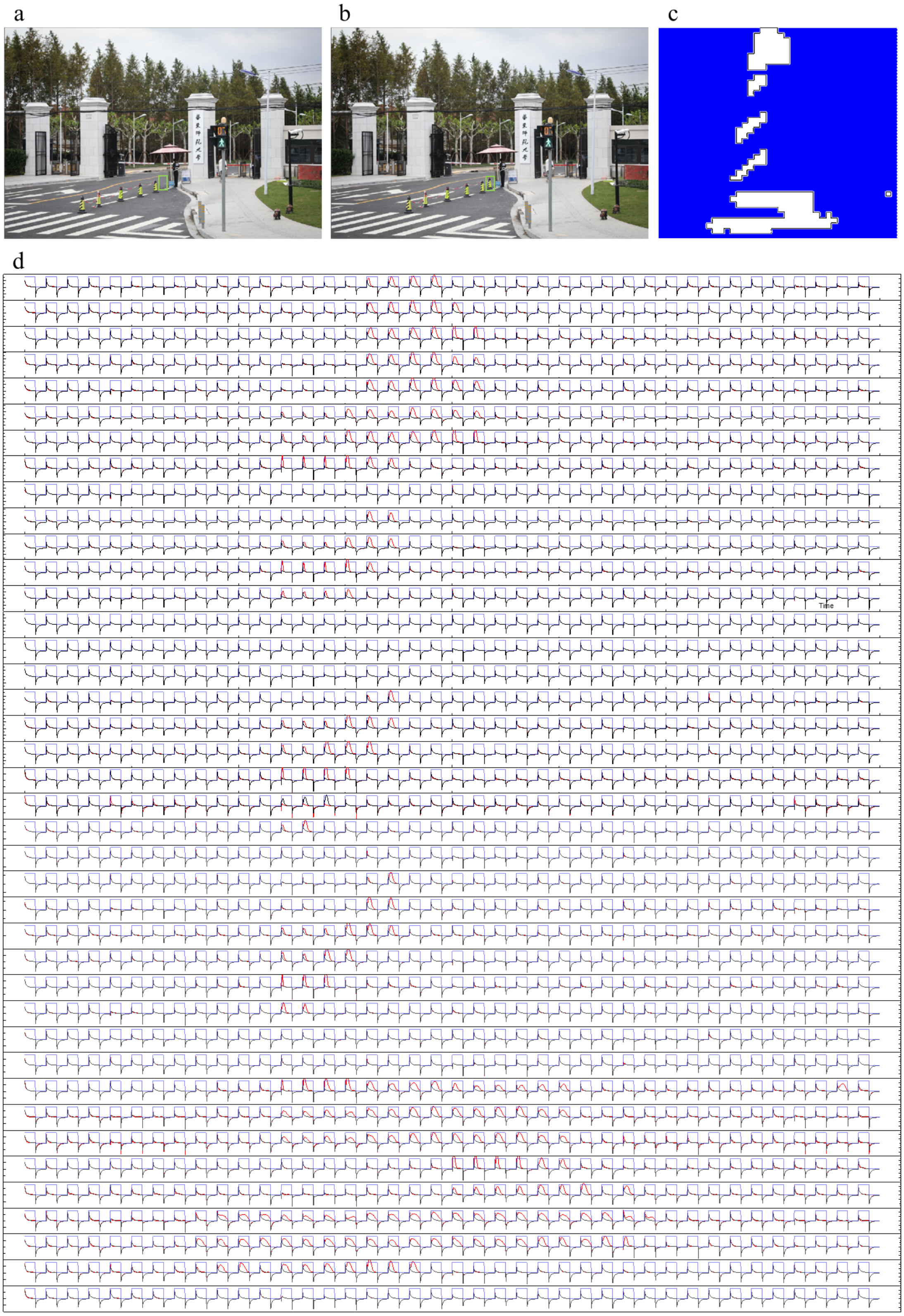

Figure S30 Extraction of image differences using ferroelectric in-memory differentiator. **a-b**, The two images of campus gate before and after one of roadblock, highlighted by green frame is put. **c**, The display of monitored different parts of the two images using the in-memory ferroelectric differentiator. **d**, The transient current response of the ferroelectric capacitor hardware during image (**b**) processing. Source data are provided as a Source Data file.

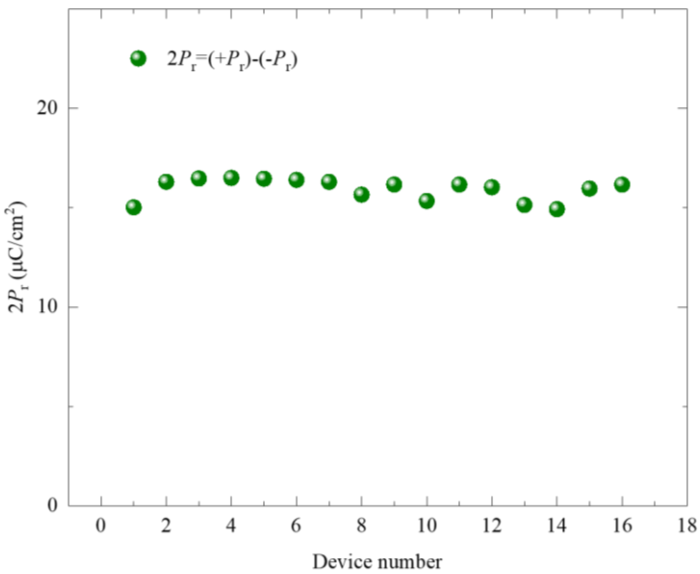

Figure S31 The variation of remanent polarization (2P_r) across 16 P(VDF-TrFE) capacitors, whose polarization versus applied electric field (*P*-*E*) curves are shown in **Fig. S3**. Source data are provided as a Source Data file.

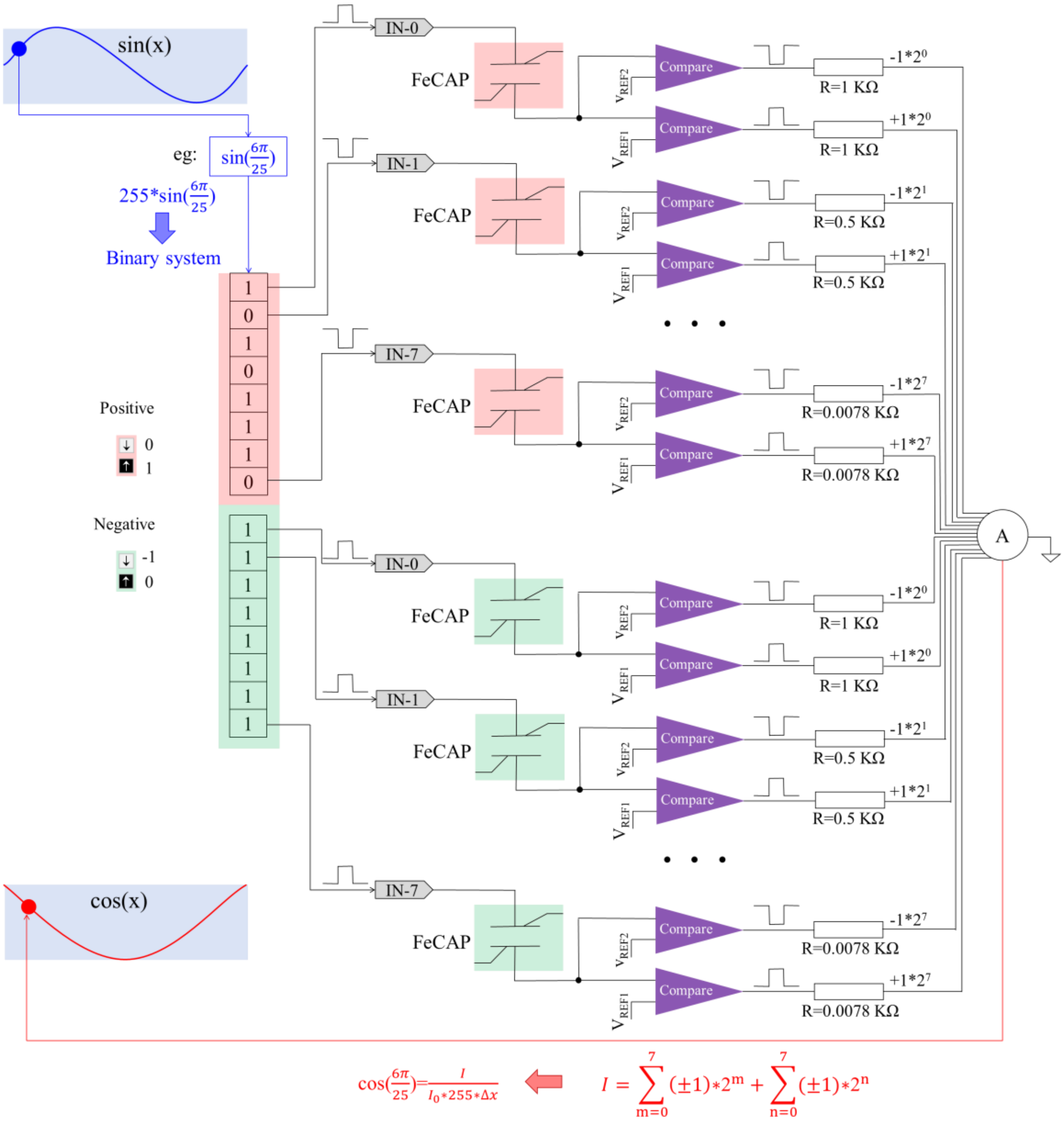

Figure S32. The ferroelectric capacitor circuits with weight coefficient for solving derivative of trigonometric functions. Only 16 capacitors can simulate any values between -1 and 1 with a resolution step of 1/255 and calculate difference value between arbitrary two dights among them.

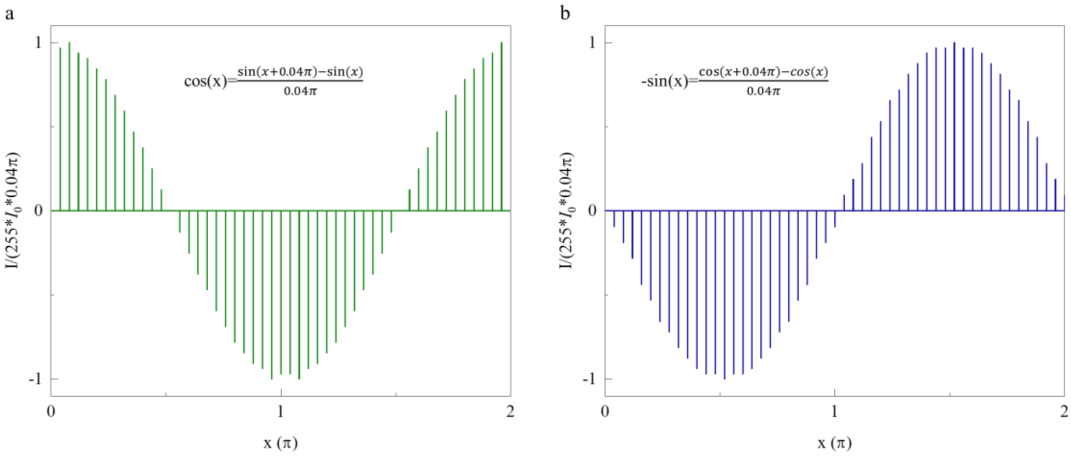

Figure S33. The first- (**a**) and second- (**b**) order derivative solution of a sine function is successfully demonstrated using the 16 binary-format ferroelectric capacitors in **Fig. S32**. Source data are provided as a Source Data file.